

The eROSITA DR1 variability catalogue

Th. Boller^{1*}, M. Freyberg¹, J. Buchner¹, F. Haberl¹, C. Maitra¹, A. Schwobe³, J. Robrade², A. Rau¹, I. Grotova¹, S. Waddell¹, Q. Ni¹, M. Salvato¹, M. Krumpke³, A. Georgakakis⁴, A. Merloni¹, and K. Nandra¹

¹ Max-Planck-Institut für extraterrestrische Physik, Gießenbachstraße 1, 85748 Garching, Germany

² Hamburger Sternwarte, Universität Hamburg, Gojenbergsweg 112, 21029 Hamburg, Germany

³ Leibniz-Institut für Astrophysik Potsdam (AIP), An der Sternwarte 16, 14482 Potsdam, Germany

⁴ National Observatory of Athens, I. Metaxa & V. Pavlou, P. Penteli, 15236, Athens, Greece

Received January 26, 2024; accepted

ABSTRACT

The extended ROentgen Survey with an Imaging Telescope Array (eROSITA) on board the Spectrum-Roentgen-Gamma (SRG) mission with its first All-Sky Survey (eRASS1) has offered an unprecedented, comprehensive view of the variable X-ray sky. With enhanced sensitivity, broader energy coverage, and improved resolution compared to prior surveys, the eRASS1 Data Release 1 (DR1) catalogue underwent a variability analysis, focusing on a substantial subset of 128,669 sources, all exhibiting a net count exceeding 10.

We performed multiple variability tests, utilizing conventional normalized excess variance (NEV), maximum amplitude variability (AMPLMAX), and Bayesian excess variance methods (bexvar). The analysis focused on binned light curves, specifically employing one eroday (a great circle scan with a duration of 4 hours) binning during the first eROSITA all-sky survey. Among the 128,669 DR1 sources, our research identified 557 objects exhibiting variability through NEV and AMPLMAX tests. After applying suitable thresholds, 108 sources demonstrated significant variability via NEV, while 73 did so through AMPLMAX. The utilization of the bexvar method extended our detection capabilities to lower count rates, unveiling a total of 1307 sources manifesting variability. We have identified objects exhibiting very high count rates that are influenced by pile-up, leading to artificial variability. Additionally, when we applied a 10-second binning to all DR1 light curves, we observed only a few sources showing significant variability, primarily due to larger error bars compared to those obtained with the eroday binning method.

Furthermore, our comparative analysis spanning 2.5 years encompassed observations from consecutive eROSITA surveys — eRASS2, eRASS3, eRASS4, and eRASS5. Nearly all DR1 sources displayed variability beyond the 3σ level across the survey scans. We computed Spearman's rank correlation coefficient for all survey mean count rates, revealing a growing count of objects as the coefficient values decreased.

We identified distinct variability patterns within specific object classes. Notably, the Gamma-ray burst afterglow GRB 200120A, which was the most variable DR1 source, was as expected absent in subsequent eROSITA survey scans.

Observations of the Low-Mass X-ray Binary GX 339–4 across various eROSITA survey scans unveiled substantial variability. In DR1, GX 339–4 showed brightness, was absent in eRASS2, and then reappeared in eRASS3 and eRASS4. These outbursts involve the movement of the inner radius of the accretion disk, fluctuating inward (reaching up to ISCO) and outward. Combining eROSITA and MAXI data reveals that the most effective tracer for monitoring the onset of the outbursts is the softest eROSITA band.

Magnetically active stars are commonly found among the more variable X-ray sources and quite often burst-like flare events are seen from otherwise faint or undetected objects. Examples include the star UCAC4 190-003482 that remained inactive throughout the eRASS1 observations except for the last scan, where it exhibited a sudden increase, reaching a count rate of 30 cts s^{-1} or the M dwarf G 124–44 where a similar event was detected.

We analyzed the AGN sample to identify variability patterns and instances of efficiency limit violations.

Key words. X-rays: general – X-rays: individuals – surveys

1. Introduction

The eROSITA telescope (Merloni et al. 2012; Predehl et al. 2021), developed by MPE and launched in 2019, provides the first complete all-sky survey in the 0.2–8 keV band. It has superior energy resolution compared to ROSAT (Truemper 1982) and shows similar sensitivity to *XMM-Newton* in soft X-rays. The initial eROSITA all-sky survey (eRASS1) delivers an extensive and unparalleled view of variable X-ray sources spanning the entire sky. This survey not only surpasses the flux, energy coverage, and resolution of previous X-ray all-sky missions but also marks a significant leap forward in survey variability studies.

In this study, we extensively explore the intricate X-ray variability, specifically concentrating on the eRASS1 light curves acquired from the eROSITA mission. This comprehensive analysis of the eRASS1 data enables a detailed examination of the temporal behaviour of X-ray emissions in both coronal stellar and accreting compact object systems. Our study relies on the utilization of the initial data release from eROSITA (DR1), as compiled by Merloni et al. (2024). From this comprehensive catalogue, we carefully selected and analyzed a substantial subset consisting of sources with a net count exceeding 10, resulting in a sizable sample of 128,669 sources for our investigation.

To ensure the integrity of our analysis and avoid any potential overlap, we have judiciously excluded the region around the south ecliptic pole (SEP) from our investigation. This particular

* E-mail: bol@mpe.mpg.de

region is being studied extensively in separate research efforts, as detailed in the works by [Bogensberger et al. \(2024\)](#) and [Liu et al. \(2024\)](#).

2. Observations and data preparation

The eRASS1 scan rate is 90 degrees per hour (i.e., a full great circle in 4 hours, which is defined as one eroday). As a result, each source moves across the field of view (FOV) in up to 40 s, with revisits occurring at an average interval of around 14,400 s. Typically, six consecutive scans are conducted over locations within the survey area and integrating over these scans is referred to as one eroday binning. In addition, we have employed a more refined approach by examining light curves using a binning interval of 10 s. This specialised technique facilitates detecting short-duration events, such as rapid 10-second variability episodes, thus broadening our understanding of the underlying variability mechanisms at play.

To conduct our analysis, the eRASS1 event file underwent meticulous processing and cleaning procedures, as detailed in the work by [Brunner et al. \(2022\)](#). From this refined event file, light curves for all 128,669 sources have been extracted. We analysed the light curves created in the eSASS pipeline for version number c010 ([Brunner et al. 2022](#); [Merloni et al. 2024](#)) by combining the telescopes with on-chip filters in the (0.6–2.3) keV band. Details on survey light curve data preparations are given in the eFEDS variability paper ([Boller et al. 2022](#)).

3. Method

3.1. eROSITA variability tests

In the following, we analyse the variability properties of the eRASS1 point sources. This includes the normalised excess variance (NEV, [Edelson et al. 1990](#); [Nandra et al. 1997](#); [Edelson et al. 2002](#)), maximum amplitude variability ([Boller et al. 2016a,b](#)), and the Bayesian excess variance ([Buchner et al. 2022](#)).

3.2. Visual screening of the variable DR1 source content

We visually screened all variable sources (see Sect. 5) and found that 10% of the sources were split by the detection software into multiple sources. Consequently, these split sources were removed from the list of variable DR1 sources.

4. Results

4.1. The most variable eRASS1 objects

In Fig. 1, we illustrate some of the most variable sources within eRASS1, arranged by decreasing AMPLMAX or NEV significance values.

The most variable source is the X-ray afterglow of the gamma-ray burst GRB 200120A detected with Fermi/GBM. The object 1eRASS J090827.6–702615 (em01_137159_820_LightCurve_00002_c010) exhibits the highest NEV significance value of all DR1 sources with $NEV = (13.39 \pm 1.57) \sigma$. On UTC Jan 20th 2020 at 23:18:15 (820 s after the Fermi/GBM trigger) [Weber \(2020\)](#) detected a bright and quickly fading X-ray source. The actual length of the observations of the afterglow in the eRASS1 all-sky survey is about 40 s, as indicated in the top left panel of Fig. 1 where a bin size of one eroday is applied, e.g. summing up four

subsequent 10 s count rate intervals. No significant variability within these 40 s is detected. The second most variable source is the Low-Mass X-ray binary system GX 339–4 (1eRASS J170249.6–484725). However, the allegedly high variability of GX 339–4 during the eRASS1 observations is most likely faked and caused by pile-up as discussed in Sect. 4.5. The third most variable source is Cen X–3 (1eRASS J112114.8–603723). SMC X–1 (1eRASS J125048.1–732630) shows a drop at the end of the eRASS1 observations which is due to an eclipse from a B0 supergiant (see Sect. 4.4).

A description of the other sources displayed in Fig. 1 is given in Table 1.

4.2. Notes on cataclysmic variables in the DR1 eRASS1 sample

We have performed a positional match between the variability catalogue and the latest edition of the CV (cataclysmic variable) catalogue by Ritter & Kolb (RKcat; [Ritter & Kolb 2003](#)) using a maximum distance between the DR1 X-ray position and the position given in the RKcat of 60'' and found 16 matches. The maximum positional offset found was 5.6'', indicating no spurious match. The matching sources can be subclassified as 10 magnetic CVs (5 intermediate polars, 5 polars), 5 dwarf novae (2 SU UMa, 2 U Gem, 1 Z Cam subtype), and one non-magnetic nova-like object of the VY Scl subtype. All but two were formerly detected in the RASS. The prevalence of the magnetic objects in the small sample is due to their intrinsic short-term variability on the orbital or the spin period of the accreting white dwarfs.

The observed pattern in the light curves reflects the folding of the intrinsic variability with the sampling period of the spacecraft. Intrinsic variability happens during the orbital period and is caused by eclipses, self-eclipses and perhaps other geometrical effects plus variations in the instantaneous mass accretion rate, which may give flares or at least non-repetitive brightness at a given spin or orbital phase. The sampling pattern may thus lead to irregular and in some cases very regular brightness variations in DR1. A nice example of a regular light curve with a simple on/off pattern is that of 1eRASS J031130.6–315250 (em01_048123_020_ML00001_002_c010), an AM Herculis star or polar with a binary orbital period of 0^d05872. The implied DR1 period of about 24 hours is much longer and occurs likely on some beat frequency between the orbital period of the CV and the scan period of the *SRG* spacecraft (see e.g. [Maitra et al. 2023](#), for another striking example of such an apparent long-period variability of an ultra-compact double degenerate binary).

4.3. Notes on the stellar DR1 variable content

Stellar sources play a significant role in the observed X-ray variability, contributing a substantial portion to it. Especially coronal emitters that generate X-rays by magnetic activity are known to be highly variable and about two-thirds of the variable sources within eRASS1 are identified as stellar by a cross-match with the eRASS DR1 stellar counterparts catalogue ([Freund et al. 2023](#), submitted). Many flare stars, young active stars and active binaries like RSCVn systems are found among the more variable sources. Several add to the most variable eRASS sources listed in Table 1, exemplary light curves of stellar sources are shown in Fig. 1 and some prominent examples are discussed below.

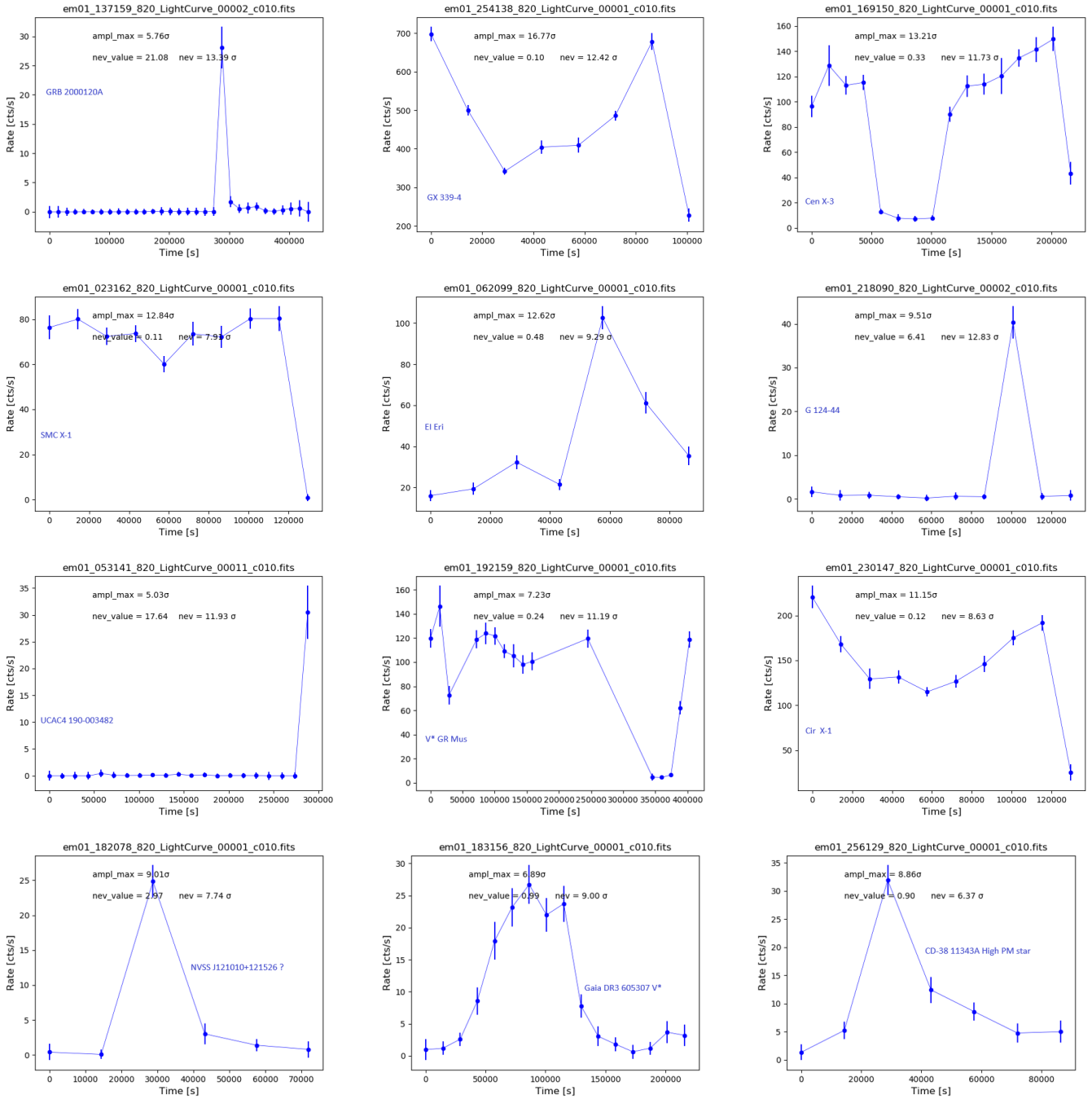


Fig. 1. Light curves of the 12 most variable DR1 sources. The bin size is one eroday, and the energy range is (0.6–2.3) keV. The objects are ordered from top left to right bottom in descending maximum amplitude σ values. For the normalised excess variance and the maximum amplitude variability, the values in units of σ are indicated along the top of each panel. The large variability of GX 339–4 is caused by pile-up.

The most variable stellar object is the RSCVn variable V* EI Eri, see Fig. 1 for its light curve. The source is bright with about 20 cts s^{-1} for about 40 ks, followed by an increase up to 100 cts s^{-1} and a subsequent decrease in count rate. Frequent flaring and highly variable X-ray emission is also reflected in its long-term variability between the eROSITA survey scans eRASS1–5 (c.f. Fig 7).

Persistent, but highly variable X-ray emission is frequently observed from nearby, X-ray bright stellar sources. Many of these are active binaries, but this type of light curve is also commonly seen in young active stars like AB Dor, which is likewise among the most variable eRASS sources.

The second most variable stellar object is the eruptive variable star G 124–44, a mid M dwarf at a distance of about 20 pc. During the eRASS1 observations, the object is mostly faint with very low count rates, except for a pronounced single flare reaching a count rate of about 40 cts s^{-1} . A similar event is seen on UCAC4 190-003482, which remained inactive throughout the eRASS1 observations except for the last eRASS scan, where it exhibited a sudden brightness increase, reaching a count rate of 30 cts s^{-1} .

These burst-like, strong but short flaring events typically occur on timescales of minutes up to an hour and thus mostly produce highly elevated count rates in single eRASS scans (c.f.

Table 1. List of the most variable eRASS1 sources ordered by descending maximum amplitude values

ID	RA ^a	Dec ^a	NEV ^b	AMP ^c	filename	ID	1eRASS name
1	137.131075	-70.437507	21.08±1.57	22.84±3.96	137159_00002	GRB 200120A	J090827.6–702615
2 ^d	255.707000	-48.790300	12.42±0.01	16.77±5.84	254138_00002	GX 339–4 LMXB	J170249.6–484725
3	170.312041	-60.623101	0.33±0.03	13.21±9.88	169150_00001	Cen X–3 HMXB	J112114.8–603723
4	19.270050	-73.441678	0.11±0.01	12.84±5.65	023162_00001	SMC X–1 HMXB	J0117048–732630
5	62.419545	-7.892090	0.48±0.05	12.62±6.20	062099_00001	EI Eri, V*	J040940.6–075531
6	216.984404	-0.372464	6.41±0.50	9.51±3.75	218090_00002	G 124–44, Eruptive Variable	J142756.2–002221
7	55.050110	-52.119301	17.64±1.48	5.03±4.97	053141_00011	UCAC4 190-003482, Star	J034012.0–520709
8	194.404642	-69.287564	0.24±0.02	7.24±7.05	192159_00001	GR Mus, LMXB	J125737.1–691715
9	230.167608	-57.165865	0.12±0.01	11.15±5.56	230147_00001	Cir X–1 HMXB	J152040.2–570957
10	182.512313	12.253138	7.74±0.38	9.01±2.42	182078_00001	NVSS J121010+121526	J121002.9+121511
11	183.313172	-64.876348	9.00±0.11	6.89±3.19	183156_00001	Gaia DR3 6053076566, V*	J121315.1–645235
12	254.203048	-39.094481	6.37±0.14	8.86±3.00	256129_00001	CD-38 11343, Eruptive Variable	J165648.7–390540
13	235.598335	-52.386520	6.29±0.09	8.62±2.51	238141_00001	Nor X–2	J154223.6–522311
14	241.408992	-20.663358	7.64±0.68	5.59±4.85	241111_00005	2MASS J16053815-2039469, YSO	J160538.1–203948
15	135.527713	-40.554228	7.06±0.05	7.47±4.99	136132_00001	Vela X–1	J090206.6–403315
16	88.371340	-81.948087	7.17±0.23	7.25±2.37	090171_00001	HD 42270, Eruptive Variable	J055329.1–815653
17	82.184945	-65.448020	4.99±0.01	2.57±1.20	080156_00002	AB Dor, V*	J052844.3–652653
18	84.859806	-69.755959	2.07±0.09	1.64±6.86	082159_00206	YSO?	J053925.3–694521
19	84.642664	-68.884785	–	1.64±1.96	082159_00007	HD 26921, Star	J053834.2–685305

Notes:

^a Units in degrees for J2000.^b Normalised excess variability in units of σ ^c Maximum amplitude variability in units of σ ^d The variability is caused by a pile-up (c.f. Sect. 4.5)

Fig. 1). Late-type stars, like the here shown M dwarfs, are frequently identified as their originating sources.

Flaring and active periods may also be present for longer timescales of hours to days, eRASS observed examples include the variable star Gaia DR3 6053076566300433920 as well as the nearby M dwarf binary CD-38 11343. Both belong to the most variable DR1 objects, their light curves are likewise shown in Fig. 1.

These findings are similar to the eFEDS variability search of Buchner et al. (2022) and Boller et al. (2022) or described in a detailed analysis of eROSITA scan analysis on the η Chamaeleontis cluster is given by Robrade et al. (2022). Notably, several early-type O/B stars exhibit distinct X-ray variability, a systematic eROSITA survey of Be stars by Nazé & Robrade (2023) presents several examples.

4.4. Notes on X-ray binaries in the DR1 variability sample

The high AMPLMAX value obtained for the high-mass X-ray binary SMC X–1 is caused by a drop in flux in the last data point of the eRASS1 light curve (see Fig. 1). In SMC X–1, a neutron star orbits a B0 supergiant, which eclipses the X-ray source regularly every 3.89 days, the binary orbital period of the system (Falanga et al. 2015). Using the ephemeris from Falanga et al. (2015), we obtain an orbital phase of -0.0505 (phase 0 corresponds to mid-eclipse time) for the time of the last eRASS1 scan and -0.0933 for the scan before (which is still at the pre-eclipse flux level).

To investigate this further, we did a detailed analysis of the complete eROSITA data of SMC X–1 from eRASS1-4. To create light curves and spectra we extracted events from circular regions around the source and a nearby background region. Because of the source brightness, we chose a sufficiently large circle with $2'$ radius. The four eRASS spectra were simultaneously fitted by an absorbed two-component model, comprising of a

power law and diskbb emission. The derived unabsorbed fluxes were used to convert the count rates to X-ray luminosities. Figure 2 shows the X-ray luminosity versus time in Modified Julian Date (MJD). Similarly to eRASS1, also the last eROSITA scans of eRASS4 fall near the eclipse ingress of SMC X–1. Assuming the eclipse ingress of SMC X–1 in soft X-ray light curves starts at phase ~ -0.1 , this suggests that the extrapolated eclipse times are slightly too early in phase, i.e. the shrinking of the orbit might be somewhat smaller than predicted by the ephemeris. Unfortunately, no egress was covered and given the uncertain eclipse duration in the eROSITA energy band, no further constraints can be derived.

4.5. Pile-up analysis for the GX 339–4 DR1 light curve

In Fig. 3 we show the soft (0.3–2 keV) and (hard 2.3–5 keV) light curves of GX 339–4. Both light curves are strongly affected by pile-up. This is obvious from the MAXI light curve (lower panel) in the 2–4 keV band which is constant within the errors as shown in the lower panel. A detailed study and summary of pile-up caused by high photon flux for the eROSITA detection of YZ Reticuli is given by König et al. (2022).

4.6. Notes on AGN variables in the DR1 eRASS1 sample

About 10% of the variable DR1 sources are classified as AGN. Table 2 lists the variable AGN candidates from the DR1 sample. In Table 2 the variable DR1 AGN content down to AMPLMAX values of 0.51σ are listed. The DR1 light curves for PKS 0558–504 and PKS 0447–439 are shown in Fig. 5.

The most variable AGN is PKS 0558-504 with an AMPLMAX value of $3.45 \pm 2.43 \sigma$ and an NEV value of $1.97 \pm 0.03 \sigma$. The source shows a drop in count rate by a factor of about 3 within about 14 hours typical for BL Lac sources. The

Table 2. List of the most variable eRASS1 AGN sources ordered by descending maximum amplitude and NEV values

Filename	RA ^a	Dec ^a	AMP ^b	NEV ^c	mult ^d	dist ^e	NAME
090141_00001	89.946827	-50.448333	3.45 ± 2.43	1.97 ± 0.03	1	3.37	PKS 0558–504
203123_00001	203.975033	-34.296359	2.50 ± 3.51	1.83 ± 0.06	1	7.61	MCG -06.30.015
072135_00001	72.352285	-43.836126	2.18 ± 3.00	2.21 ± 0.02	1	1.94	PKS 0447–439
079123_00001	79.89885	-32.658446	1.71 ± 2.86	1.85 ± 0.06	1	3.53	ESO 362-G18
056111_00001	55.514588	-21.245037	1.45 ± 2.73	1.28 ± 0.07	1	5.31	ESO 548-G81
155069_00002	155.877614	19.865086	1.25 ± 3.17	0.82 ± 0.04	1	1.73	NGC 3227
035141_00001	32.339889	-52.489316	1.14 ± 2.22	0.21 ± 0.05	1	0.85	RXS J02093–5229
067138_00001	69.366745	-47.191497	1.11 ± 2.15	–	1	0.91	RXS J04374–4711
171081_00001	172.054247	10.386239	1.06 ± 1.47	0.96 ± 0.66	1	3.47	SDSS J11282+1023
176129_00001	174.758255	-37.738585	0.95 ± 4.08	0.39 ± 0.01	1	2.15	NGC 3783
087147_00001	85.987495	-55.535344	0.93 ± 4.12	0.35 ± 0.01	1	2.66	RXS J05439–5532
183060_00003	184.611228	29.812703	0.91 ± 1.74	0.25 ± 0.12	1	2.83	MARK 766
078075_00001	77.689184	16.498836	0.80 ± 2.44	–	1	1.82	2E 0507+1626
059159_00001	58.240157	-68.521430	0.76 ± 2.14	–	1	0.25	PKS 0352–686
188147_00005	190.358225	-57.835379	0.75 ± 1.55	–	1	16.79	WKK 1263
169126_00002	168.140261	-36.425578	0.67 ± 1.50	–	1	15.51	ESO 377-G24
053126_00002	53.40069	-36.140514	0.67 ± 1.68	–	1	3.38	NGC 1365
093147_00002	92.322929	-56.116626	0.67 ± 1.92	–	1	1.21	CTS H34.06
167114_00001	165.90675	-23.492317	0.66 ± 3.34	–	1	1.73	H 1101–232
172132_00001	170.201355	-43.264186	0.64 ± 2.43	–	1	4.64	ESO 265-G23
208108_00001	207.874124	-18.230096	0.58 ± 1.92	–	1	5.71	CTS J13.12
226105_00001	225.920262	-15.687400	0.51 ± 1.12	–	1	2.43	RXS J15037–1541

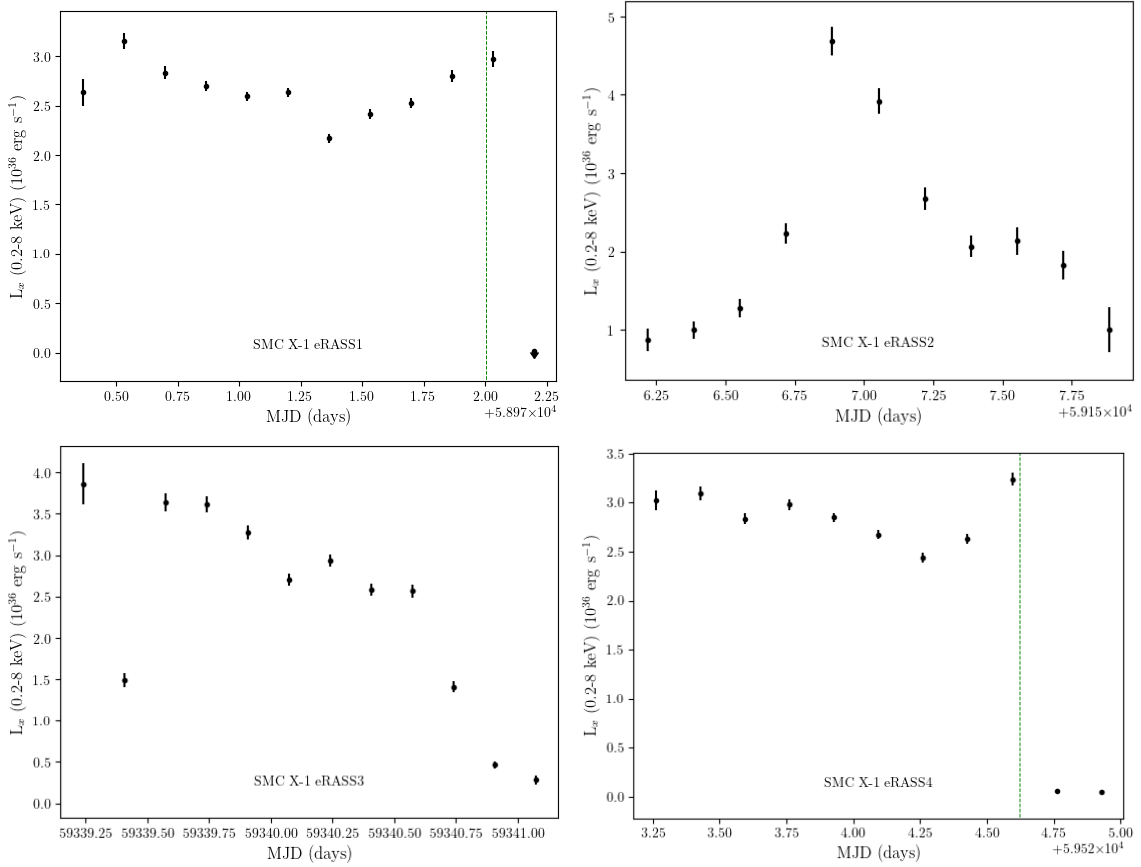
Notes:

^a Units in degrees.

^b Maximum amplitude variability in units of σ .

^c Normalised excess variability in units of σ .

^d Number of counterparts within the search radius.

^e Angular distance between the DR1 catalogue position and the Veron & Veron catalogue in arcseconds.

Fig. 2. eROSITA light curves of SMC X–1. Count rates were converted into X-ray luminosity using parameters from spectral modelling and a distance of 65 kpc. The vertical dashed lines mark an orbital phase of -0.1, the expected start of eclipse ingress.

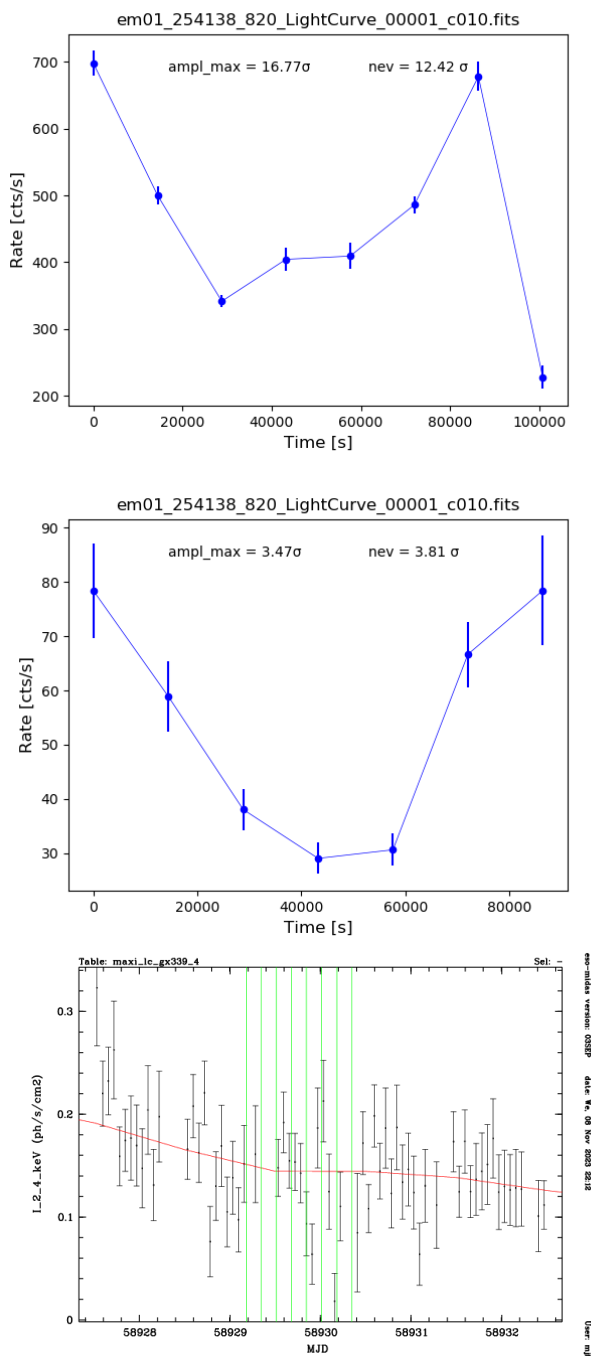


Fig. 3. The DR1 light curves of GX 339–4 in the soft (top panel) and hard (middle panel). Both light curves are affected by pile-up causing artificial variability. Lower panel: MAXI lightcurves in the (2–4) keV band, in black the "orbit" (1.5h) and in red the "1day" data values. The green vertical lines indicated the 4 eRASS survey periods. Within the error bars the MAXI light curve is constant during the eRASS1 observations, in contrast to the eRASS1 soft and hard light curves, most probably due to strong pile-up in the eROSITA bands.

efficiency limit was not violated during the eRASS1 observations.

The second most variable AGN is the largely studied source MCG-06-30-015. The DR1 variability is moderate with about 10% count rate variations, while between the eROSITA survey observations, a factor of 1.5 variability is detected.

PKS 0447–439 shows variations by a factor of up to 4 during the DR1 observations. The source is also highly variable between the eROSITA survey observations.

5. The eRASS1 variability catalogue

Within the 128,669 DR1 sources, our research pinpointed 557 showing variability with significance values surpassing 0σ values in both NEV and AMPLMAX tests.

After applying suitable thresholds (Buchner et al. 2022), 108 sources demonstrated significant variability via NEV, while 73 did so through AMPLMAX. The utilization of the *bevxar* method extended our detection capabilities to lower count rates, unveiling a total of 1307 sources manifesting variability (c.f. Fig. 6). This is less than about 1% of the complete DR1 catalogue.¹

6. Comparison of variable DR1 sources with eRASS2, 3, 4 and 5 observations

6.1. Overall variability and Spearman's rank analysis

We have compared the DR1 sources which show variability with the eRASS2, 3, 4, and 5 observations by comparing their mean count rates. The timescale which is tested covers about 2.5 years starting with the 2019 eRASS1 observations until the 2022 eRASS5 observations which were stopped on February 26th. A fraction of 96% of the DR1 sources is variable above the 1σ level. Some sources are not detected in individual survey scans while others remain detected through the eRASS1–5 observations. We note that the GRB 200120A detected during eRASS1 is not detected in subsequent eRASS2–5 observations, as expected from such types of sources. Another example of variability on the half-year time scale is Vela X–1 with count rates of about 44, 13, 0.8, and 5 cts s^{-1} (middle panel in Fig. 7). In Fig. 8 the distribution of the AMPLMAX and NEV values for DR1 sources detected in eRASS2 to eRASS5 surveys are shown.

We have computed the Spearman's rank coefficient for all individual survey light curves. These coefficients were grouped to intervals from 1 to -1. We find an increasing number of sources with decreasing Spearman's rank coefficients (c.f. Fig. 9). Detailed studies of long-term variability of eRASS sources are being performed aimed at identifying interesting extragalactic nuclear transients (such as Tidal Distruption Events, Changing Look AGN, etc.). These will be reported elsewhere (Grotova et al. (2024); Bahic et al. (2024)).

6.2. Analyzing GX 339–4: Combining eROSITA and MAXI Data for Physical Insights

The Low-Mass X-ray Binary (LMXB) GX 339–4 shows significant X-ray variability between the eROSITA survey scans initially bright in eRASS1, followed by a non-detection in eRASS2, and then reappearing during eRASS3 and eRASS4 (see Fig. 7, upper left panel).

In Fig. 4 we compare the MAXI count rates in different energy bands with the eROSITA count rates in surveys eRASS1,2,3,4. The MAXI light curve is depicted across different energy intervals, ranging from the MAXI soft (2–4 keV)

¹ Table of the DR1 sources with variability test results is only available in electronic form at the CDS via anonymous ftp to cdsarc.u-strasbg.fr (130.79.128.5)

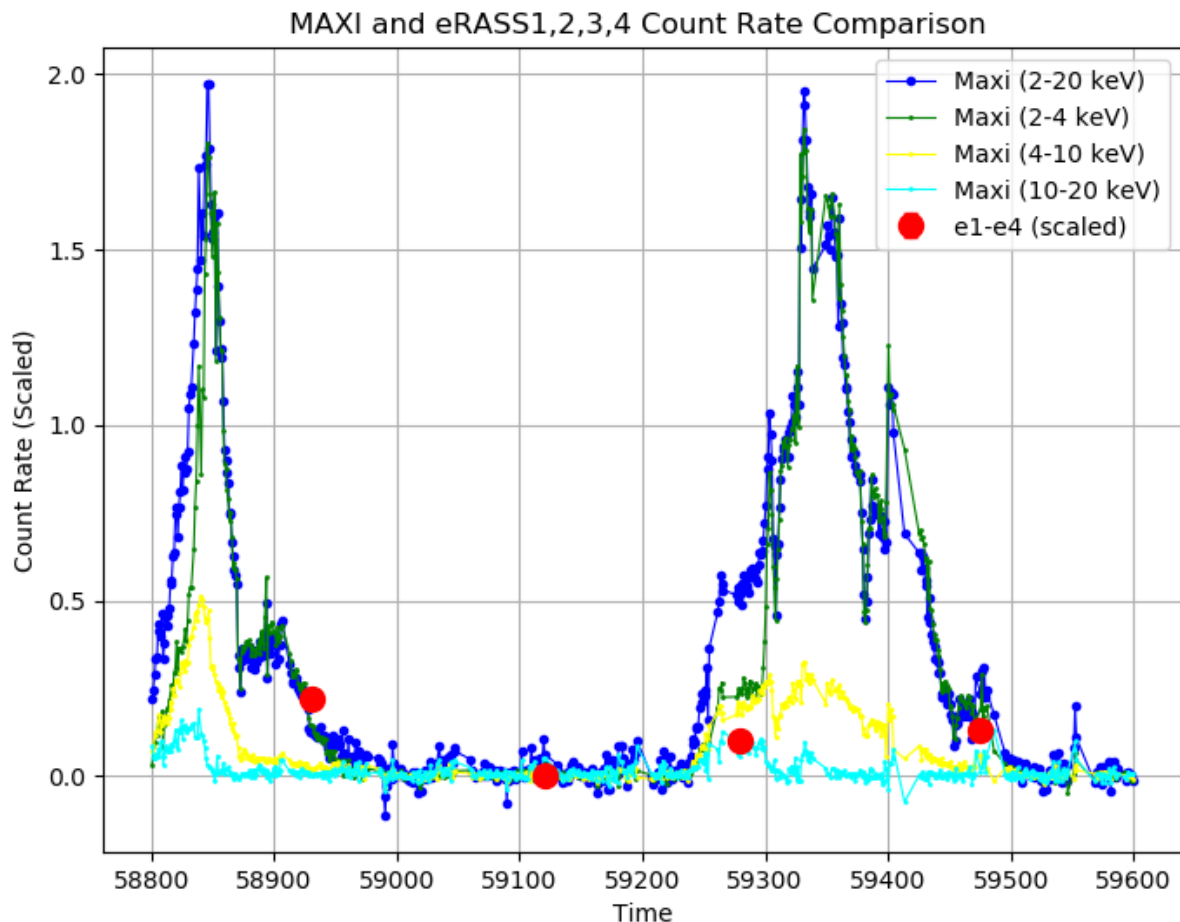


Fig. 4. Overlay of eRASS1, 2, 3, and 4 soft band (0.6–2.3 keV) count rates on the MAXI data in the 2–20 keV (blue), 2–4 keV (green), 4–10 keV (yellow), and 10–20 keV (cyan) energy range for the source GX 339–4. The eRASS1–4 data points are scaled to the MAXI count rate value in the 2–20 keV band for the time interval of the eRASS1 observation.

through the MAXI middle (4–10 keV) to the MAXI hard (10–20 keV), including the total MAXI (2–20 keV) energy range. It’s noteworthy that the MAXI hard band precedes the count rate peak emission, while the MAXI middle and MAXI soft bands exhibit later peaks with increasing intensity during the onset of the flares. This consistency aligns with the interpretation of black body emission, a decreasing innermost stable orbit (ISCO) value of the accretion disc with increasing intensity during the flare onsets [Fabian et al. \(1982\)](#). The ISCO resides proximate to the Galactic black hole in the MAXI soft band and extends outward in the MAXI middle and MAXI hard energy bands.

We scaled the eRASS1,2,3,4 count rates against the total MAXI band count during the initial eRASS observations. This scaling was consistent with the MAXI count rate off-state observed during eRASS2 observations. Upon doing this, we observed an offset in the eRASS3 observations compared to the MAXI soft and middle energy intervals.

The eRASS3 observations coincide with the onset of the flaring event across all the MAXI count rate energy bands. During this initial phase of the flare, we anticipate the innermost edge of the disc to transition from larger distances closer to the black hole, resulting in a shift to smaller distances. Consequently, we would expect the MAXI observations in the harder energy bands

to exhibit a greater influence on the energy release compared to observations in the softer bands. This aligns with the findings from eRASS1 observations. The alignment of the very hard (10–20 keV) count rates with those from eRASS1 is likely coincidental, primarily due to the dominance of the inversely Compton scattered power-law emission from the corona over the black body emission within this energy band. During the phase of offset, the correlation between the energy bands, their respective count rate states the time delays are not as obvious compared to the onset phase.

In summary, the softest eROSITA band proves most effective in tracking the onset of the outbursts.

7. Summary

Among the 128,669 DR1 sources, our research identified 557 exhibiting variability through NEV and AMPLMAX tests. After applying suitable thresholds, 108 sources demonstrated significant variability via NEV, while 73 did so through AMPLMAX. Utilizing the bexvar method extended our detection capabilities to lower count rates, unveiling a total of 1307 sources manifesting variability, based on a one eroday binning.

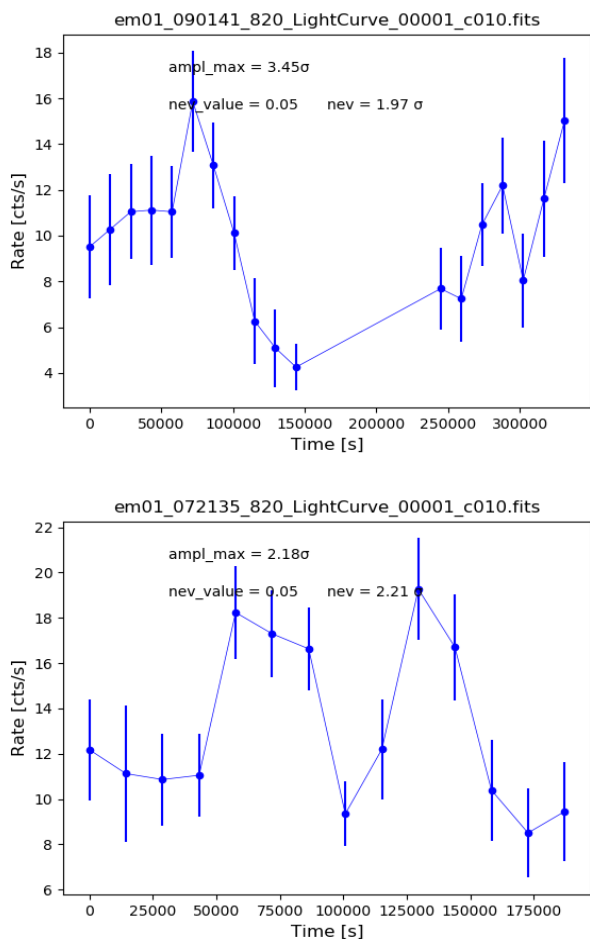


Fig. 5. Light curve examples for DR1 sources classified as AGN. The left panel shows the light curve of PKS 0558–504, and the right panel is for PKS 0447–439.

Moreover, the exploration for variability at a 10-second interval uncovered distinctive sources exhibiting variability on shorter time scales.

Notably, over 97% of these variable sources within eRASS1 displayed detectable variability in subsequent eROSITA observations (eRASS2, eRASS3, eRASS4, and eRASS5), uncovering distinct patterns within specific object classes.

For instance, as anticipated, the Gamma-ray burst GRB 2000120A, the most variable DR1 source, was absent in later eROSITA survey scans.

Observations of the LMXB GX 339–4 were conducted during the separate eROSITA survey scans. GX 339–4 exhibited significant variability, starting with brightness in DR1, followed by absence in eRASS2, and reappearing in eRASS3 and eRASS4. We compare the MAXI count rates with the eROSITA count rates in surveys 1,2,3, and 4. The eRASS3 and eRASS4 observations appear offset from the MAXI observations while eRASS1 and eRASS2 give comparable count rates. The most probable explanation for the offset between the eRASS3 and 4 count rates compared to the MAXI observations is that the sensitivity of eROSITA to lower energy levels enabled it to trace the onset or decline of the outburst effectively. These outbursts, classified as high-soft states, involve the movement of the inner radius of the accretion disk, fluctuating inward (reaching up to ISCO) and outward. Combining eROSITA and MAXI data re-

veals that the most effective tracer for monitoring the onset of the outbursts is the softest eROSITA band.

Magnetically active stars are commonly found among the more variable X-ray sources and often burst-like flare events are seen from otherwise faint or undetected objects. Examples include the star UCAC4 190-003482 that remained inactive throughout the eRASS1 observations except for the last data point, where it exhibited a sudden increase, reaching a count rate of 30 cts s⁻¹ or the M dwarf G 124–44 where a similar event was detected.

We analyzed the AGN sample to identify variability patterns and instances of efficiency limit violations.

Acknowledgements. This work is based on data from eROSITA, the soft X-ray instrument aboard *SRG*, a joint Russian-German science mission supported by the Russian Space Agency (Roskosmos), in the interests of the Russian Academy of Sciences represented by its Space Research Institute (IKI), and the Deutsches Zentrum für Luft- und Raumfahrt (DLR). The *SRG* spacecraft was built by Lavochkin Association (NPOL) and its subcontractors, and is operated by NPOL with support from the Max Planck Institute for Extraterrestrial Physics (MPE). The development and construction of the eROSITA X-ray instrument was led by MPE, with contributions from the Dr. Karl Remeis Observatory Bamberg & ECAP (FAU Erlangen-Nuernberg), the University of Hamburg Observatory, the Leibniz Institute for Astrophysics Potsdam (AIP), and the Institute for Astronomy and Astrophysics of the University of Tübingen, with the support of DLR and the Max Planck Society. The Argelander Institute for Astronomy of the University of Bonn and the Ludwig Maximilians Universität Munich also participated in the science preparation for eROSITA." The eROSITA data shown here were processed using the eSASS/NRTA software system developed by the German eROSITA consortium. MK acknowledges support from DLR FKZ 50OR2307.

References

- Bahic et al., S. 2024, A&A, in prep.
 Bogensberger et al., D. 2024, A&A, in prep.
 Boller, T., Freyberg, M. J., Trümper, J., et al. 2016a, A&A, 588, A103
 Boller, T., Freyberg, M. J., Trümper, J., et al. 2016b, A&A, 588, A103
 Boller, T., Schmitt, J. H. M. M., Buchner, J., et al. 2022, A&A, 661, A8
 Brunner, H., Liu, T., Lamer, G., et al. 2022, A&A, 661, A1
 Buchner, J., Boller, T., Bogensberger, D., et al. 2022, A&A, 661, A18
 Edelson, R., Turner, T. J., Pounds, K., et al. 2002, ApJ, 568, 610
 Edelson, R. A., Krolik, J. H., & Pike, G. F. 1990, ApJ, 359, 86
 Fabian, A. C., Guilbert, P. W., Motch, C., et al. 1982, A&A, 111, L9
 Falanga, M., Bozzo, E., Lutovinov, A., et al. 2015, A&A, 577, A130
 Freund, S., Czesla, S., Predehl, P., et al. 2023, A&A, subm.
 Grotova et al., J. 2024, A&A, in prep.
 König, O., Wilms, J., Arcodia, R., et al. 2022, Nature, 605, 248
 Liu et al., T. 2024, A&A, in prep.
 Maitra, C., Haberl, F., Vasilopoulos, G., et al. 2023, A&A, subm.
 Merloni, A., Predehl, P., Becker, W., et al. 2012, arXiv e-prints, arXiv:1209.3114
 Merloni et al., A. 2024, A&A, in press
 Nandra, K., George, I. M., Mushotzky, R. F., Turner, T. J., & Yaqoob, T. 1997, ApJ, 476, 70
 Nazé, Y. & Robrade, J. 2023, MNRAS, 525, 4186
 Predehl, P., Andritschke, R., Arefiev, V., et al. 2021, A&A, 647, A1
 Ritter, H. & Kolb, U. 2003, A&A, 404, 301
 Robrade, J., Czesla, S., Freund, S., Schmitt, J. H. M. M., & Schneider, P. C. 2022, A&A, 661, A34
 Truemper, J. 1982, Advances in Space Research, 2, 241
 Weber, P. 2020, GRB Coordinates Network, 26988, 1

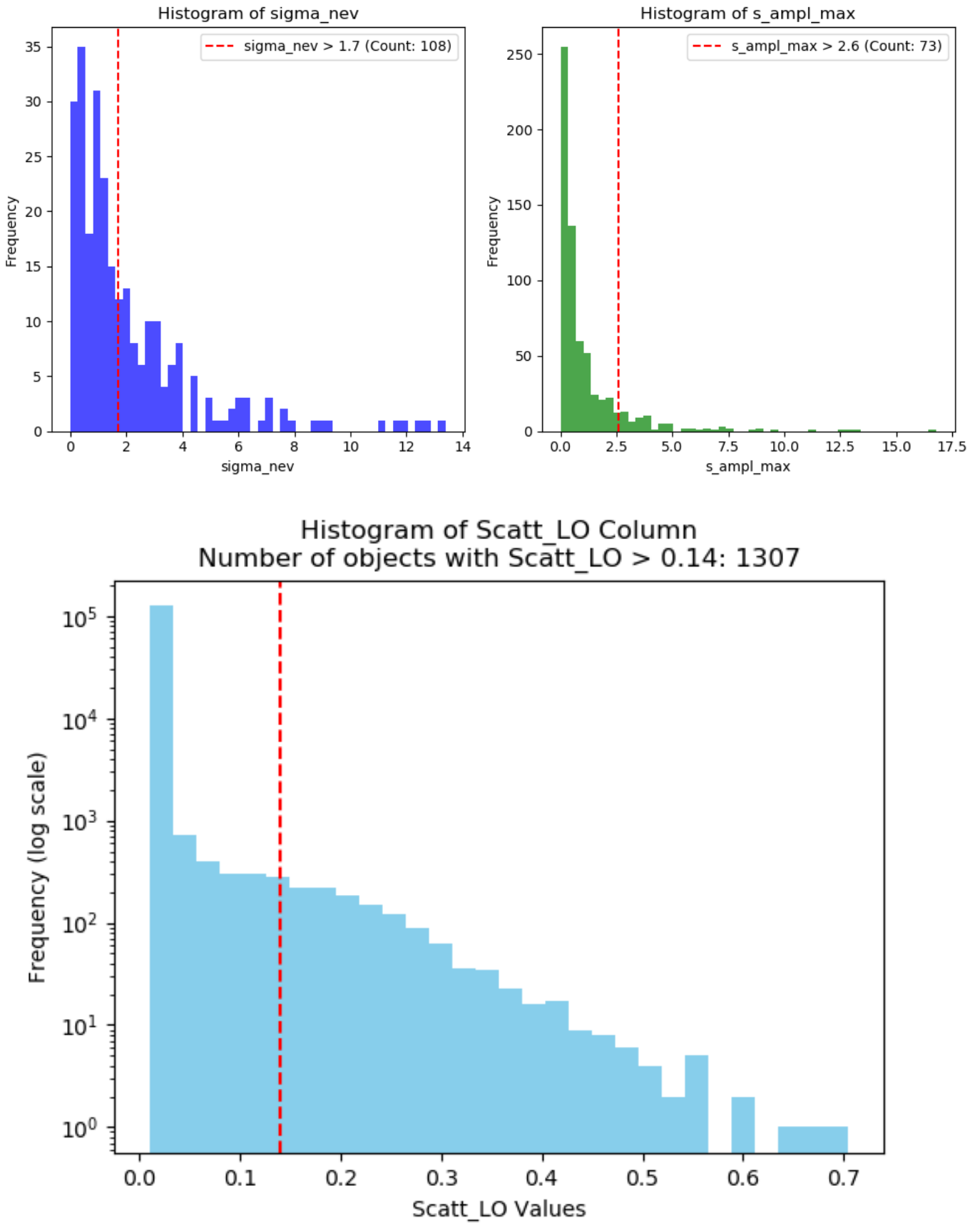


Fig. 6. Upper panels: Histograms of the NEV and AMPLMAX significance distributions. Sources with NEV values greater than 1.7 sigma and AMPLMAX values greater than 2.6 σ (red dashed lines) are considered variable DR1 objects. Lower panel: Histogram of the bexvar results for the unbinned data. Sources with scatter low values greater than 0.14 σ (red dashed line) are considered variable DR1 objects.

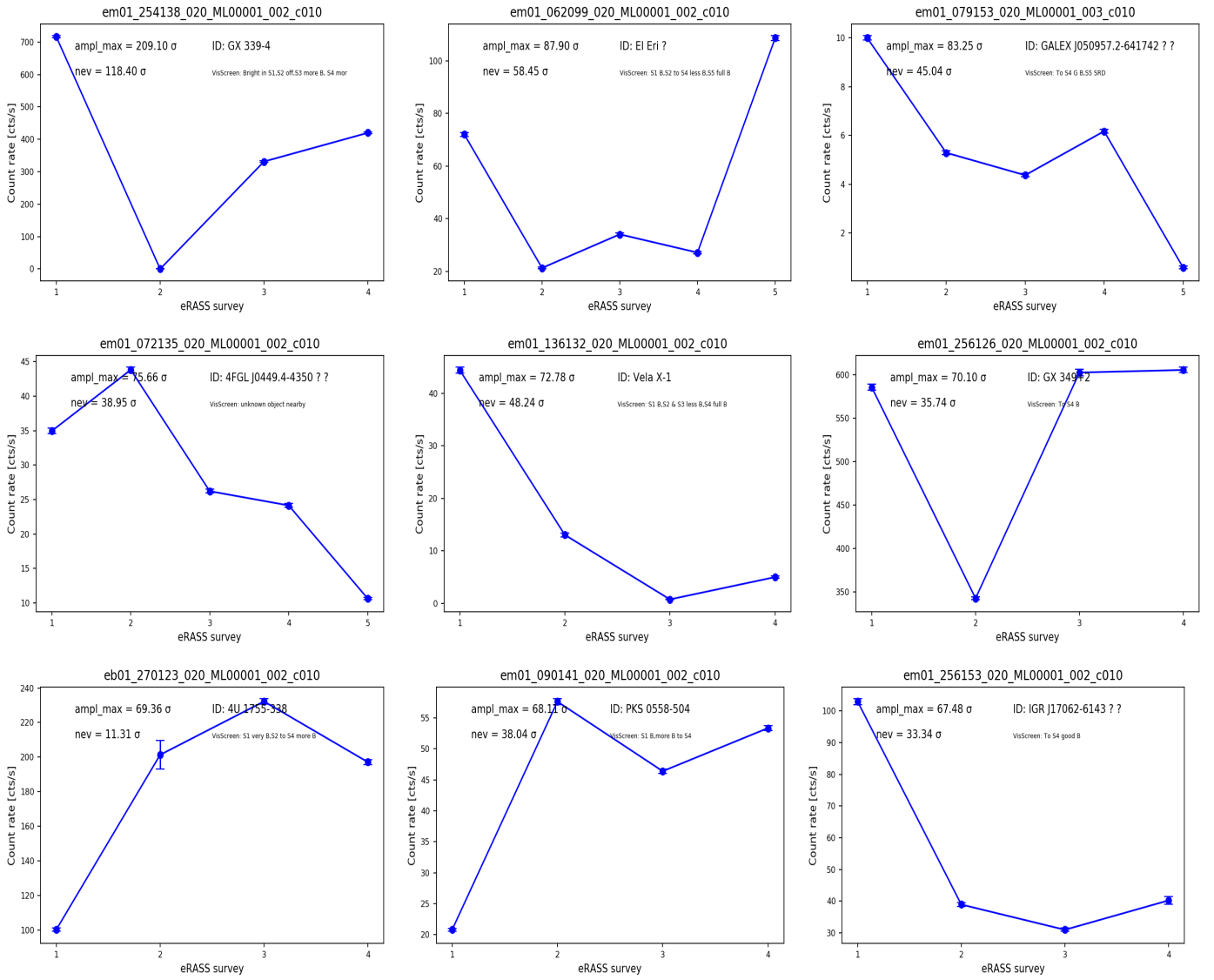


Fig. 7. DR1 sources with high variability significance levels between the individual eROSITA surveys. The labels on the top of the figures refer to the DETUID entry in the DR1 catalogue.

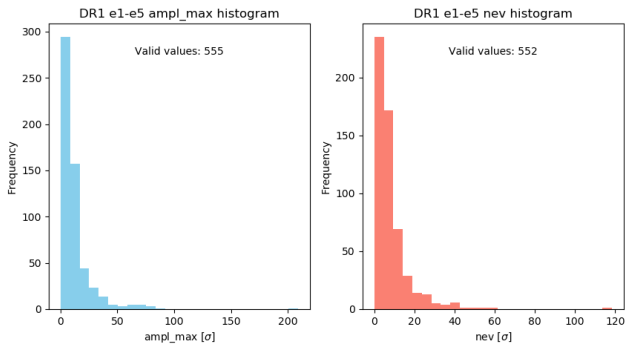


Fig. 8. Histograms of DR1 sources detected in eRASS2,3,4,5 observations. The plots show the histograms of amplmax and nev in units of σ . More than 95% of the DR1 sources with intrinsic variability show variability over a time scale of 2.5 years.

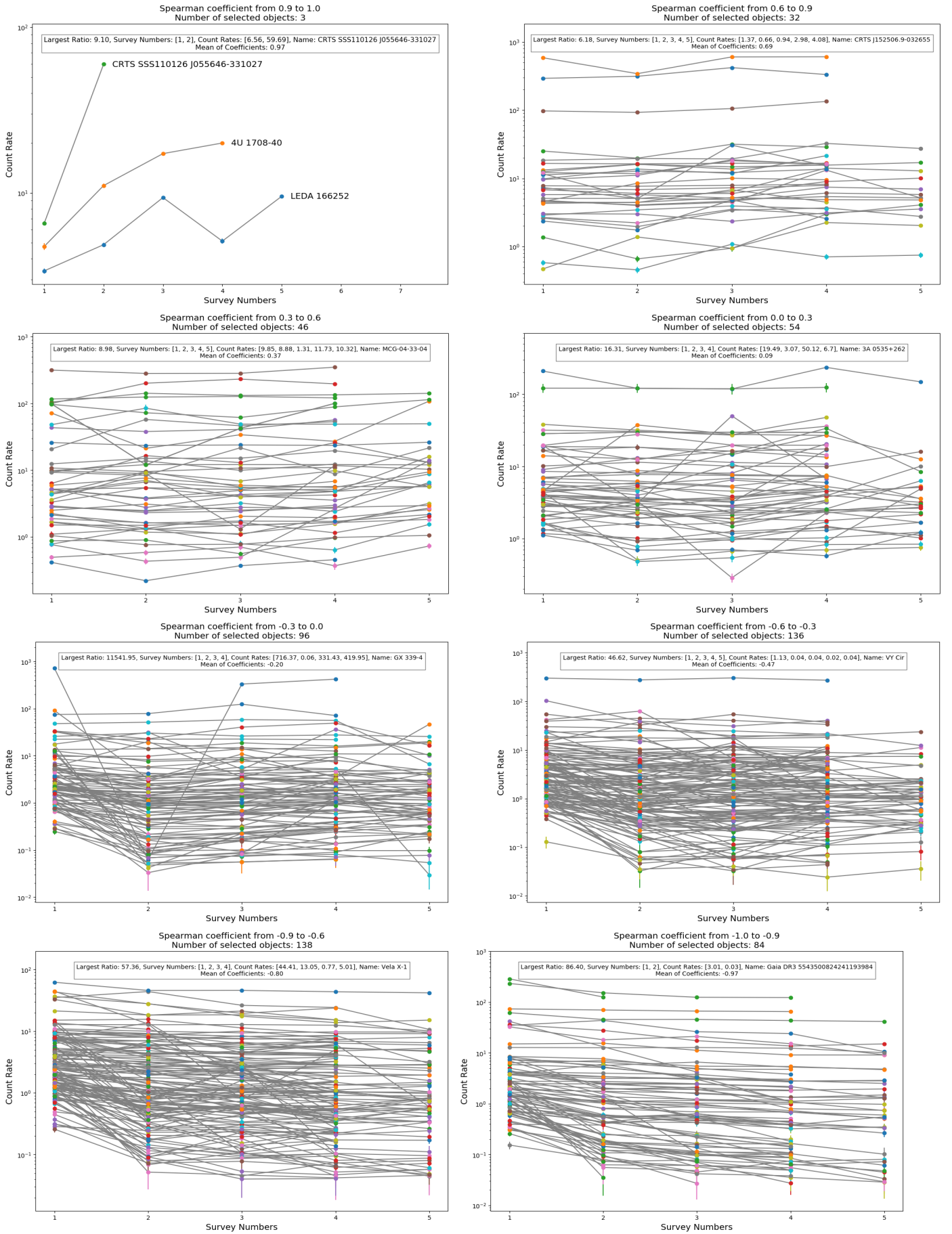


Fig. 9. Spearman Rank coefficient distributions plotted in descending order. The number of objects is increasing towards lower coefficients. This is expected as primarily DR1 sources are compared to their eRASS survey fluxes in subsequent epochs.

Appendix A: Search for variability on the 10 s level

In addition to the variability analysis based on the eroday binning we have analysed the variability on the eSASS light curve products binned with 10 s, c.f. Fig. A.1. The smaller inlay in the figures shows the total light curve. Source 136132_00001 (135.5376,-40.5291) is identified as Vela X-1 an HMXB. A count rate drops by about a factor of 2 within 40 s from about 70 down to about 30 cts s^{-1} . The source is also listed in Table 1 with significant variability based on the eroday binning. The data set 254148_00001, which represents GX 339-4, shows artificial variability caused by substantial pile-up for both the eROSITA day and the 10-second binning. 077162_00001 is LMC X-2, a highly variably source with DR1 which also shows AMPLMAX variability at the 3.5σ level at the 10 second level. 023162_00001 is SMC X-1. There is a drop from 100 down to about 60 cts s^{-1} within 20 s. The last data point in the DR1 light curve shown in the inlay is due to occultation. 317135_00003 is a multiple-star system HD 199388. The most significant variability is found with 4 data points jumping up and down with nearly identical low and high count rate states. 316141_00003 is the galaxy ESO 235-50 with a redshift of 0.048, not detected in X-rays so far. 245105_00048 is the star HD 146935 with a G magnitude of 8.44. 082159_00004 is associated with OGLE LMC-SC7 468632, a RR Lyrae variable object. The most significant and most interesting variability pattern occurs at about 76208 s with a quasi-periodic jump down in count rates.

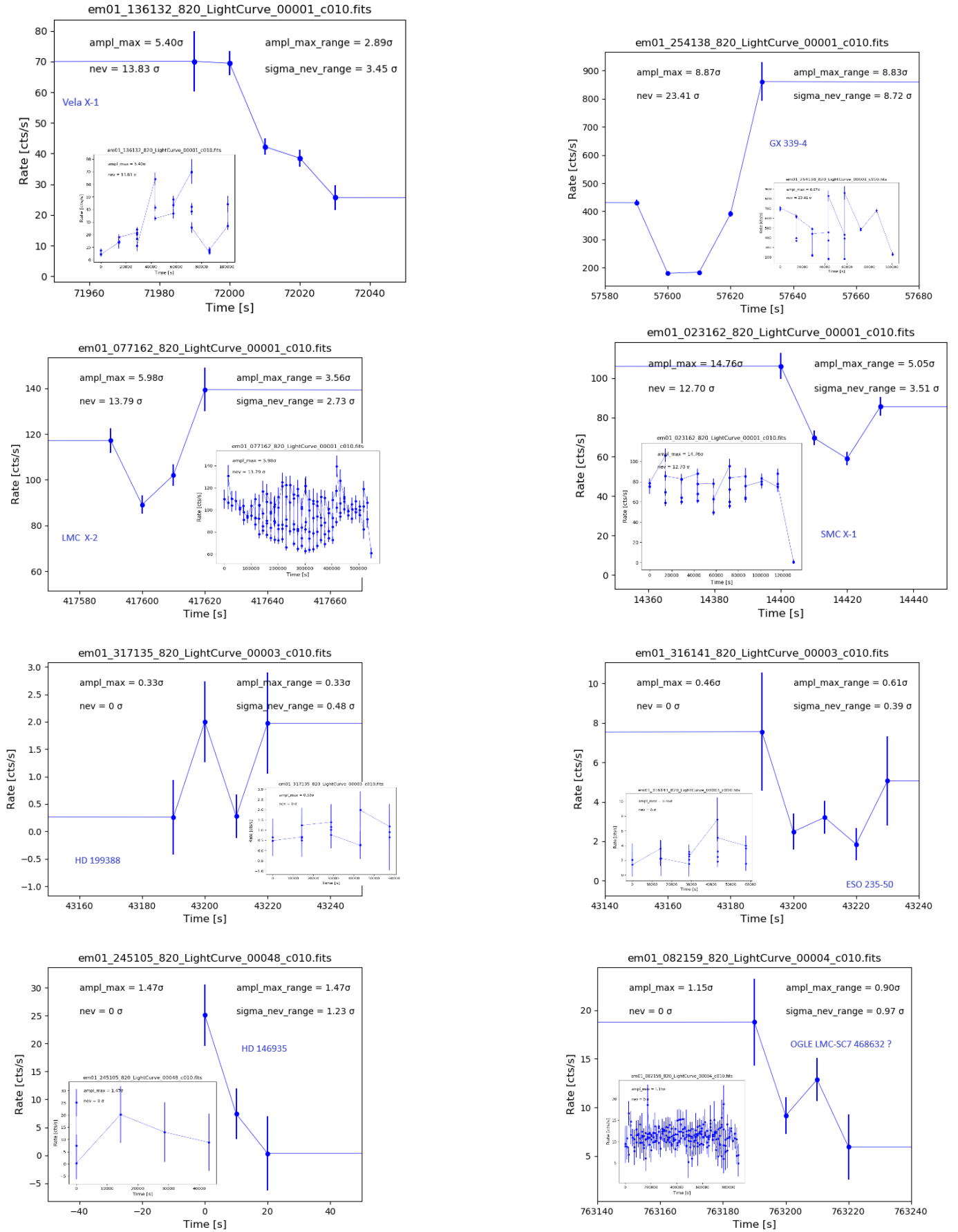


Fig. A.1. Sources exhibiting variability on a 10-second timescale are depicted, with the most variable segment of the light curve highlighted. The complete light curve is presented in the insets.